PAPER

Check for updates

Tuning the exposure of BiVO$_4$-{010} facets to enhance the N$_2$ photofixation performance†

Honghao Chu,[a] Shisheng Zheng,[a] Yang Li,[a] Kuanda Xu,[a] Qingshui Hong,[b] Tangyi Li,[a] Wenju Ren,[c] Shunning Li,[a] Zongwei Mei[*a] and Feng Pan [ID] [*ad]

Effective separation of photoexcited carriers and chemisorption of the N$_2$ molecule are two key issues to efficient nitrogen photofixation. The spatial charge separation of BiVO$_4$ with anisotropic exposed facets, namely the transfer of photoexcited electrons and holes to {010} and {110} facets, respectively, helps to enhance the separation ability of photogenerated carriers. Theoretical calculation results predict that a surface oxygen vacancy is easier to form on the (010) facet than on the (110) facet of BiVO$_4$. Accordingly, in this study, enhanced N$_2$ photofixation performance has been achieved for the first time by tuning the exposure of {010} facets of BiVO$_4$.

Nitrogen fixation to NH$_3$ is an important artificial synthesis in the chemical industry.[1] Nowadays, NH$_3$ is commonly produced through the Haber–Bosch process, which requires high temperature (400–500 °C) and high pressure (15–25 MPa).[2] This process accounts for ∼2% of the total global energy consumption and contributes ∼1.6% of the total global emissions.[3] With the growing energy needs and demand for cleaner environment, a more environmentally friendly method is needed for NH$_3$ manufacture. Photocatalytic N$_2$ fixation, which employs solar energy and water to produce ammonium, is a promising sustainable and green strategy for NH$_3$ synthesis compared with the traditional Haber–Bosch process.[4–9] However, the photocatalytic performance of N$_2$ fixation is far from satisfactory due to the inefficient separation of photogenerated carriers, the high activation energy barriers and hard cleavage of the strong N≡N triple bond energy (941 kJ mol^{-1}) of the N$_2$ molecule.[10]

Crystal facet engineering of semiconductors is a significant strategy for fine-tuning the charge separation of photocatalysts.[11] Facet engineering of anatase TiO$_2$ has been given considerable research attention for photocatalytic reaction by controlling the {001} exposure ratio.[12–14] Recently, different research groups reported that the exposure of anisotropic facets of BiOX (X = Cl, Br, or I) enabled the directional transfer of photoexcited electrons and holes for spatial charge separation,

accordingly improved the photocatalytic activities.[15–17] Other semiconductors including SrTiO$_3$,[18] LaNbON$_2$,[19] and C$_3$N$_4$ (ref. 20) also demonstrated that the predominating anisotropic facet exposure could improve the separation of photogenerated carriers. Simultaneously, the spatial charge separation of BiVO$_4$ with anisotropic exposed facets has been observed by direct imaging[21] and photo-reduction or photo-oxidation reactions on {010} or {110} facets, respectively.[22–24] These results indicated that the photoexcited electrons (e$^-$) and holes (h$^+$) would transfer to the {010} and {110} facets, respectively. Based on the special property of BiVO$_4$, photocatalytic water splitting for O$_2$ evolution has been greatly improved.[25] However, a few researches on BiVO$_4$ with anisotropic exposed facets have been reported for photocatalytic N$_2$ fixation.

It is commonly understood that surface vacancies with abundant localized electrons play a critical role in N$_2$ photofixation by capturing and activating the inert N$_2$ molecule.[26,27] Efficient transfer of the photogenerated electrons to the inert N$_2$ molecule is also a key step for the effective photocatalytic N$_2$ fixation.[28] Considerable research results have revealed that surface oxygen vacancies could activate the N$_2$ molecule by chemisorption, and act as the transfer bridge of photoexcited electrons from photocatalysts to the activated N$_2$ molecule. For example, Pan et al. reported that the bond length of N≡N was elongated by the interaction with the surface O$_{VS}$ on MoO$_{3-x}$ nanobelts or W$_{18}$O$_{49}$ nanowires, and the photocatalytic activities for the N$_2$ fixation were directly related to the surface O$_{VS}$ concentration.[29,30] The critical role of O$_{VS}$ in the photofixation of N$_2$ was also revealed by other semiconductors including TiO$_2$,[10,31–33] BiOCl,[34] BiO quantum dots,[35] ultrafine Cu$_2$O,[8] and amorphous CeO$_x$.[36] However, the surface O$_{VS}$ on BiVO$_4$ for N$_2$ photofixation has been rarely studied.

Theoretical calculation results predicted that the formation energy (E_f) of an O$_V$ on the surface of the representative (010)

^{a}School of Advanced Materials, Peking University, Shenzhen Graduate School, Shenzhen, China. E-mail: meizw@pkusz.edu.cn; panfeng@pkusz.edu.cn

^{b}Chongqing Key Laboratory of Chemical Process for Clean Energy and Resource Utilization, School of Chemistry and Engineering, Chongqing University, Chongqing, China

^{c}School of Advance Manufacturing Engineering, Chongqing University of Posts and Telecommunications, Chongqing, China

^{d}Chemistry and Chemical Engineering Guangdong Laboratory, Shantou, China

facet was lower than that on the surface of the typical (110) facet, accordingly there were more O_{VS} on the surface of the (010) facet. Together with the spatial charge separation property, anisotropic exposed $BiVO_4$ was believed to exhibit a good N_2 photofixation performance. In this study, $BiVO_4$ with anisotropic {010} and {110} facets were synthesized by a solid–liquid state reaction.[37] It was first found that the as-prepared $BiVO_4$ with higher percentage of exposed {010} facets exhibited better performance for N_2 photofixation without any sacrificial reagent and cocatalyst under ambient conditions. The easier formation of a surface oxygen vacancy (O_V) on the (010) facet was experimentally proved by the enhanced chemisorption of the N_2 molecule based on the temperature programmed desorption (TPD) characterization. The enhanced separation of photogenerated carriers and more surface oxygen vacancies (O_{VS}) made $BiVO_4$ with a higher exposed ratio of {010} facets to be more efficient for photocatalytic N_2 fixation.

The primitive unit cell consists of four units as shown by the side and top view of the optimized $BiVO_4$ (Fig. 1a and b), and the optimized lattice parameters are as follows: $a = 7.33$ Å, $b = 11.77$ Å, $c = 5.18$ Å, and $\beta = 134.92°$. They are in good agreement with the experimental values: $a = 7.25$ Å, $b = 11.70$ Å, $c = 5.09$ Å, and $\beta = 134.225°$. The formation energy of the oxygen vacancy (E_f) on the surface of (010) and (110) facets were calculated by following equation:

$$E_f = E_{O_V} + E_{\frac{1}{2}O_2} - E_{surface}$$

where E_{O_V}, $E_{\frac{1}{2}O_2}$, and $E_{surface}$ represent the total energy of surface with one oxygen vacancy, the half of total energy of oxygen and the total energy of surface without oxygen vacancy. The calculated formation energies of an oxygen vacancy were 2.91 eV and 4.93 eV on (010) and (110) surface, respectively. It means that the formation of a surface oxygen vacancy on the (010) facet was more energetically favorable than that on the (110) facet.

Based on the theoretical calculation result, $BiVO_4$ with different exposure ratios of {010} facets was fabricated by tuning the nitric concentration in the reaction solution according to a previous report (see ESI†). The as-synthesized $BiVO_4$-0.50, $BiVO_4$-0.75, and $BiVO_4$-1.0 can be indexed to the monoclinic crystal structure (PDF# 14-0688) (Fig. 2a and S1†). However, the $BiVO_4$-0.25 sample in Fig. S1† consists of a hybrid monoclinic structure (PDF# 14-0688) and a tetragonal crystal phase (PDF# 14-0133), probably due to the low concentration of the HNO_3 solution. Furthermore, the (020) peak of $BiVO_4$-0.50 appears around 15° of 2θ (Fig. 2a). The as-synthesized $BiVO_4$ in different concentrations of HNO_3 shows different facet exposure ratios of {010} to {110}, and $BiVO_4$-0.50 exhibits the largest exposure ratio (Fig. 2b and S2†), which is consistent with the previous report.[37] The largest exposure of {010} facets must cause the appearance of the (020) peak in Fig. 2a. The typical TEM image shows the regular shape of $BiVO_4$-0.50 (Fig. 2c). The HRTEM interplanar spacing is 0.47 nm, corresponding to the value of (110) facet (Fig. 2d). The selected area electron diffraction (SAED) rings in the inset of Fig. 2d corresponds to the (110) and (040) crystal facets of monoclinic $BiVO_4$.

Fig. 3 exhibits the temperature programmed desorption (TPD) characterization of the N_2 molecule. A single peak centering at 220 °C is observed, which is ascribed to the desorption of the chemisorbed N_2, and $BiVO_4$-0.50 exhibits the strongest chemisorption of the N_2 molecule. It is consistent with the theoretical calculation result shown in Fig. 1.

For the general photocatalytic N_2 photofixation process in pure water, the photoexcited electrons are injected into the
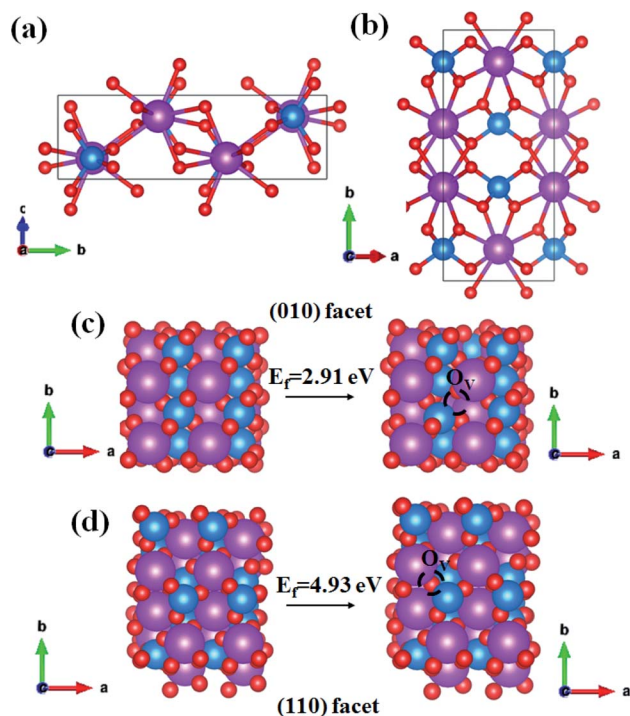

Fig. 1 The side view (a) and top view (b) of optimized monoclinic $BiVO_4$. The purple, blue and red atom indicates Bi, V and O, respectively; (c) the optimized structure of the (010) surface and (010) surface with one vacancy. (d) The optimized structure of the (110) surface and (110) surface with one vacancy.
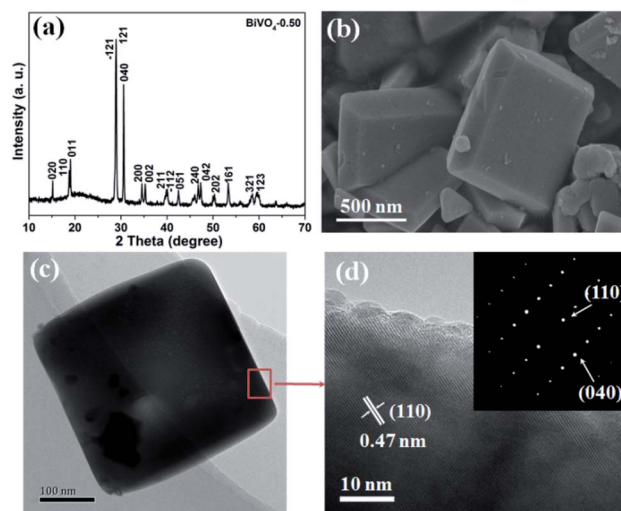

Fig. 2 Typical XRD pattern (a), SEM image (b), TEM image (c), and HRTEM image (d) of the as-synthesized $BiVO_4$-0.50. Inset in (d) SAED pattern.
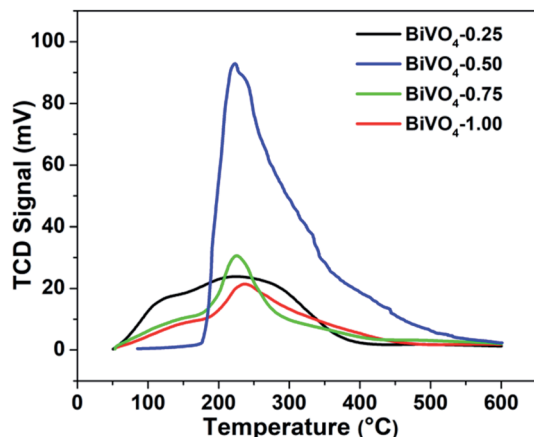
Fig. 3 N_2-TPD profiles of $BiVO_4$ synthesized in the aqueous solution with different HNO_3 concentrations.

Fig. 5 Photocatalytic stability test for $BiVO_4$-0.50 (light source: 300 W xenon lamp; photocatalyst: 0.05 g; reaction solution: 100 ml of pure water).

chemisorbed N_2 molecule *via* oxygen vacancy, and then the activated N_2 molecule combines with H^+ from water to form NH_3. Simultaneously, the photogenerated holes oxidize the OH^- from water to produce O_2. The standard curve from the different concentrations of NH_4^+ is shown in Fig. S4.† Photocatalytic performance test indicates that $BiVO_4$-0.50 exhibits the best activity for N_2 fixation among these four samples (Fig. 4a). The average NH_4^+ evolution rate is about 15.5 μmol g^{-1} L^{-1} h^{-1} for $BiVO_4$-0.50 during a 6 h test. The average NH_4^+ evolution rates decrease to 13.1, 5.35, and 5.3 μmol g^{-1} L^{-1} h^{-1} for $BiVO_4$-0.75, $BiVO_4$-1.00, and $BiVO_4$-0.25, respectively (Fig. 4a). The Brunauer–Emmett–Teller (BET) measurements indicate that the surface areas are 2.9 m^2 g^{-1}, 2.0 m^2 g^{-1}, 1.8 m^2 g^{-1}, and 1.5 m^2 g^{-1} for $BiVO_4$-0.25, $BiVO_4$-0.50, $BiVO_4$-0.75, and $BiVO_4$-1.00, respectively. The corresponding ratios of the average NH_4^+ evolution rate to surface area are 4.5 μmol L^{-1} h^{-1} m^{-2}, 7.8 μmol L^{-1} h^{-1} m^{-2}, 3.0 μmol L^{-1} h^{-1} m^{-2}, and 3.5 μmol L^{-1} h^{-1} m^{-2}. It is obvious that the surface area is not the determining factor of the photocatalytic activity. In order to confirm the origination of the nitrogen element in NH_4^+, Ar gas was bubbled and the aqueous suspension of the $BiVO_4$-0.50 sample was irradiated by a 300 W xenon lamp during the test time. It is found that there is no detectable NH_4^+ (Fig. 4a), and it can be concluded

that the detected NH_4^+ did not originate from environmental contamination, but from the photofixation reaction of N_2 molecule by the $BiVO_4$ photocatalyst. Fig. 4b shows the light-wavelength-dependent photofixation activity of $BiVO_4$-0.50. The photocatalytic performance decreases from 365 nm and exhibits almost no NH_4^+ from 515 nm, and no NH_4^+ is detected at 590 nm due to the light absorption range (Fig. S3†). The photocatalyst possessed photoexcited electrons with higher energy under the irradiation of the shorter wavelength light, and the photofixation of N_2 was more easy to occur. However, the photofixation reaction of N_2 molecule could not occur when the longer wavelength light was unable to excite the $BiVO_4$ photocatalyst. This result further confirmed the photofixation of N_2 in our study. The calculated value of quantum efficiency (QE) at 365 nm was about 0.003%.

In order to evaluate the stability of $BiVO_4$-0.50 for N_2 photofixation, three cycle tests were carried out, as exhibited in Fig. 5. After each cycle, the photocatalyst was washed by vacuum filtration with pure water for several times and dried in a vacuum oven. The photocatalytic activity gradually decreased probably due to the loss of photocatalyst during the wash process.

In summary, $BiVO_4$ with exposed anisotropic {010} and {110} facets was synthesized, and studied for the first time for ammonia production by photocatalytic N_2 fixation from pure water. It was found that the sample with the high facet exposure ratio of {010} to {110} exhibited a better photocatalytic performance for N_2 fixation, which resulted from the better separation ability of the photoexcited carriers and more surface O_{VS} on the {010} facet. The photoexcited electrons more effectively transferred to the more surface O_{VS} on the typical (010) facet, where the N_2 molecule can be activated, and accordingly benefited to the enhancement of the photocatalytic performance. Our study provides a good strategy to improve the photocatalytic activity for N_2 fixation.
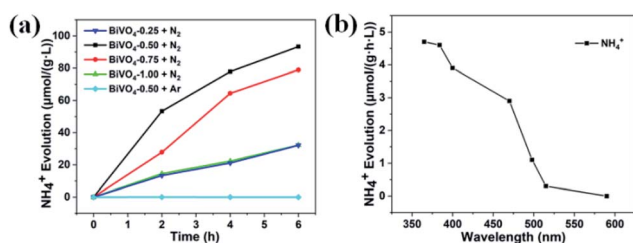

Fig. 4 (a) Photocatalytic nitrogen fixation performance of $BiVO_4$ samples synthesized with different concentrations of nitric acid (light source: 300 W xenon lamp; photocatalyst: 0.05 g; reaction solution: 100 ml of pure water). (b) Nitrogen fixation performance of $BiVO_4$-0.50 illuminated by LED with different wavelengths (365 nm, 384 nm, 400 nm, 470 nm, 498 nm, 515 nm, and 590 nm).
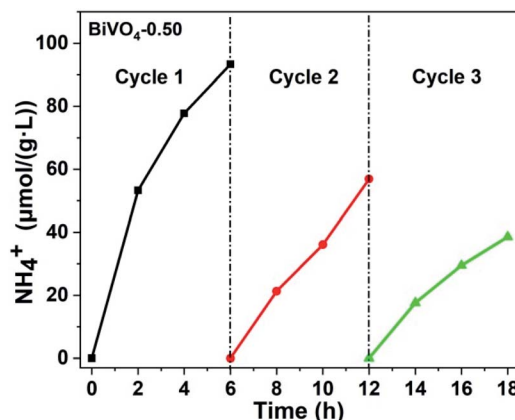
Conflicts of interest

There are no conflicts to declare.

Acknowledgements

References

1 D. E. Canfield, A. N. Glazer and P. G. Falkowski, *Science*, 2010, **330**, 192–196.

2 G. N. Schrauzer and T. D. Guth, *J. Am. Chem. Soc.*, 1977, **99**, 7189–7193.

3 P. Friedlingstein, M. O'Sullivan, M. W. Jones, R. M. Andrew, J. Hauck, A. Olsen, G. P. Peters, W. Peters, J. Pongratz and S. Sitch, *Earth Syst. Sci. Data*, 2020, **12**, 3269–3340.

4 Y. Feng, Z. Zhang, K. Zhao, S. Lin, H. Li and X. Gao, *J. Colloid Interface Sci.*, 2021, **583**, 499–509.

5 W. Gao, X. Li, S. Luo, Z. Luo, X. Zhang, R. Huang and M. Luo, *J. Colloid Interface Sci.*, 2020, **585**, 20–29.

6 X. Hu, Y. Yong, Y. Xu, X. Hong, Y. Weng, X. Wang and X. Yao, *Appl. Surf. Sci.*, 2020, **531**, 147348.

7 N. Ojha, A. Bajpai and S. Kumar, *J. Colloid Interface Sci.*, 2020, **585**, 764–777.

8 S. Zhang, Y. Zhao, R. Shi, C. Zhou, G. I. Waterhouse, Z. Wang, Y. Weng and T. Zhang, *Angew. Chem., Int. Ed.*, 2021, **60**, 2554–2560.

9 Z. Zhao, C. Choi, S. Hong, H. Shen, C. Yan, J. Masa, Y. Jung, J. Qiu and Z. Sun, *Nano Energy*, 2020, **78**, 105368.

10 H. Hirakawa, M. Hashimoto, Y. Shiraishi and T. Hirai, *J. Am. Chem. Soc.*, 2017, **139**, 10929–10936.

11 J. Bai, J. Sun, X. Zhu, J. Liu, H. Zhang, X. B. Yin and L. Liu, *Small*, 2020, **16**, 1904783.

12 L. Ruan, X. Wang, T. Wang, Z. Ren, Y. Chen, R. Zhao, D. Zhou, G. Fu, S. Li, L. Gao, Y. Lu, Z. Wang, H. Tian, X. Kong and G. Han, *ACS Appl. Mater. Interfaces*, 2019, **11**, 37256–37262.

13 T. Tachikawa, S. Yamashita and T. Majima, *J. Am. Chem. Soc.*, 2011, **133**, 7197–7204.

14 X. Han, Q. Kuang, M. Jin, Z. Xie and L. Zheng, *J. Am. Chem. Soc.*, 2009, **131**, 3152–3153.

15 M. Shi, G. Li, J. Li, X. Jin, X. Tao, B. Zeng, E. A. Pidko, R. Li and C. Li, *Angew. Chem., Int. Ed.*, 2020, **59**, 6590–6595.

16 T. Li, C. Wang, T. Wang and L. Zhu, *Appl. Catal., B*, 2020, **268**, 118442.

17 M. Li, S. Yu, H. Huang, X. Li, Y. Feng, C. Wang, Y. Wang, T. Ma, L. Guo and Y. Zhang, *Angew. Chem., Int. Ed.*, 2019, **58**, 9517–9521.

18 L. Mu, Y. Zhao, A. Li, S. Wang, Z. Wang, J. Yang, Y. Wang, T. Liu, R. Chen, J. Zhu, F. Fan, R. Li and C. Li, *Energy Environ. Sci.*, 2016, **9**, 2463–2469.

19 X. Wang, T. Hisatomi, J. Liang, Z. Wang, Y. Xiang, Y. Zhao, X. Dai, T. Takata, K. Domen and K. Domen, *J. Mater. Chem. A*, 2020, **8**, 11743–11751.

20 L. Lin, Z. Lin, J. Zhang, X. Cai, W. Lin, Z. Yu and X. Wang, *Nat. Catal.*, 2020, **3**, 649–655.

21 J. Zhu, F. Fan, R. Chen, H. An, Z. Feng and C. Li, *Angew. Chem., Int. Ed.*, 2015, **54**, 9111–9114.

22 H. Li, Y. Sun, B. Cai, S. Gan, D. Han, L. Niu and T. Wu, *Appl. Catal., B*, 2015, **170**, 206–214.

23 R. Li, H. Han, F. Zhang, D. Wang and C. Li, *Energy Environ. Sci.*, 2014, **7**, 1369–1376.

24 J. Lu, Y. Lei, K. C. Lau, X. Luo, P. Du, J. Wen, R. S. Assary, U. Das, D. J. Miller and J. W. Elam, *Nat. Commun.*, 2013, **4**, 1432.

25 D. Wang, H. Jiang, X. Zong, Q. Xu, Y. Ma, G. Li and C. Li, *Chem.–Eur. J.*, 2011, **17**, 1275–1282.

26 S. Wang, X. Hai, X. Ding, K. Chang, Y. Xiang, X. Meng, Z. Yang, H. Chen and J. Ye, *Adv. Mater.*, 2017, **29**, 1701774.

27 T. Hou, Y. Xiao, P. Cui, Y. Huang, X. Tan, X. Zheng, Y. Zou, C. Liu, W. Zhu, S. Liang and L. Wang, *Adv. Energy Mater.*, 2019, **9**, 1902319.

28 Y. Liu, M. Cheng, Z. He, B. Gu, C. Xiao, T. Zhou, Z. Guo, J. Liu, H. He, B. Ye, B. Pan and Y. Xie, *Angew. Chem., Int. Ed.*, 2019, **58**, 731–735.

29 W. Ren, Z. Mei, S. Zheng, S. Li, Y. Zhu, J. Zheng, Y. Lin, H. Chen, M. Gu and F. Pan, *Research*, 2020, 3750314.

30 Y. Li, X. Chen, M. Zhang, Y. Zhu, W. Ren, Z. Mei, M. Gu and F. Pan, *Catal. Sci. Technol.*, 2019, **9**, 803–810.

31 X. Niu, Q. Zhu, S. Jiang and Q. Zhang, *J. Phys. Chem. Lett.*, 2020, **11**, 9579–9586.

32 J. Yang, Y. Guo, R. Jiang, F. Qin, H. Zhang, W. Lu, J. Wang and J. C. Yu, *J. Am. Chem. Soc.*, 2018, **140**, 8497–8508.

33 Y. Zhao, Y. Zhao, R. Shi, B. Wang, G. I. N. Waterhouse, L. Z. Wu, C. H. Tung and T. Zhang, *Adv. Mater.*, 2019, **31**, 1806482.

34 Y. Shiraishi, M. Hashimoto, K. Chishiro, K. Moriyama, S. Tanaka and T. Hirai, *J. Am. Chem. Soc.*, 2020, **142**, 7574–7583.

35 S. Sun, Q. An, W. Wang, L. Zhang, J. Liu and W. A. Goddard, *J. Mater. Chem. A*, 2017, **5**, 201–209.

36 C. Zhang, Y. Xu, C. Lv, L. Bai, J. Liao, Y. Zhai, H. Zhang and G. Chen, *Appl. Catal., B*, 2020, **264**, 118416.

37 H. L. Tan, X. Wen, R. Amal and Y. H. Ng, *J. Phys. Chem. Lett.*, 2016, **7**, 1400–1405.